Spectroscopic Studies of Electron and Hole Trapping in Zeolites: Formation of Hydrated Electrons and Hydroxyl Radicals

Xinsheng Liu,† Guohong Zhang, and J. Kerry Thomas*

Department of Chemistry and Biochemistry, University of Notre Dame, Notre Dame, Indiana 46556

Received: September 9, 1996; In Final Form: December 3, 1996[⊗]

The trapping of electrons by water clusters and the reaction of positively charged holes in pulsed electron radiolysis of hydrated zeolites X and Y were studied using time-resolved transient absorption spectroscopy. The fully hydrated zeolites, under 12 mbar of water vapor, exhibit a short-lived structureless absorption band centered at 620 nm. This is attributed to hydrated electrons confined to the 13 Å supercages of the zeolites. The band is blue-shifted by 0.28 eV relative to that of the hydrated electrons in bulk liquid water. With the gradual removal of water molecules from the zeolite cavities, a continuous red shift of the transient absorption spectra is observed in both zeolites X and Y. The similarity of the spectral features of hydrated electrons in zeolites to those of water cluster anions in the gas phase suggests that water exists in the form of clusters in the zeolite supercages. The spectral shift with decreasing size of the water clusters presumably demonstrates that the confinement of water by the zeolite cages on the nanometer dimension affects solvation and electronic structures of the excess electrons. It is shown that water clusters trap electrons more weakly as their sizes become smaller and that cation cluster trapping sites are gradually formed during dehydration. Electron transfer from the water cluster trapping sites to the cation cluster trapping sites is clearly observed when the water content is decreased to ∼32 water molecules per pseudocell (a supercage plus a sodalite cage) in zeolites X with a Si/Al ratio of 1.0. A high radiolytic yield of $G_e = 5.8$ is measured for the water cluster trapped electrons in fully hydrated NaY. The unique transport of hydrated electrons in zeolite cages is understood in terms of an adiabatic model. The reactivity of positively charged holes generated by the ionizing radiation as geminate pairs with excess electrons is examined in both hydrated and dry zeolites. Trapping and reactions of the positive holes with aromatic molecules and water leads to the formation of organic radical cations and hydroxyl radicals, respectively. Essentially the same high yield of hydroxyl radicals as that of water cluster solvated electrons is measured in zeolite Y at the highest water content, $G_{OH^\bullet} = 6.0$. The addition reactions of $OH^\bullet$ with aromatic molecules included in zeolites is found to be limited by the slow diffusion of $OH^\bullet$ through the zeolite supercages.

Introduction

Microporous zeolites are one of the most important materials used in industry for catalysis, adsorption, and ion exchange.[1−4] The use of this type of materials is expanding, and attempts have been made on many aspects of their applications.[5−21] Studies on the trapping of electrons by charge-balancing cation clusters and by guest species in the zeolite cavities has been active in recent years due to interest in the confinement of zeolite cavities, metal-to-insulator transitions,[8,9,14] charge transfer and stabilization,[5,18] solar energy conversion,[6] and base-catalyzed reactions.[7]

The phenomenon of electron trapping by charge-balancing cation clusters, Na_4^{4+}, in zeolites was first discovered by Kasai in 1965[10] and confirmed later by Barrer et al. in 1968.[11] Over the past 10 years or so, research on this aspect of zeolites has made great progress in the understanding of the nature of the trapping sites and has led to discoveries of a variety of trapping sites containing different numbers of cation.[5,7−20] Several review articles have been published on this subject.[5,8,14]

Very recently, we found that the water in zeolite cavities could also trap electrons, forming hydrated electrons.[20] This finding has inspired us to study a rather old but still very fascinating subject, hydrated electrons. Over several decades, numerous studies on hydrated electrons present in different forms of water such as clusters,[22−24] liquid,[25,26] ice,[26] and clathrates[27] have been conducted. The studies on the gas phase water clusters have concentrated mainly on the dynamics of electron detachment and cluster dissociation after photoexcitation of water cluster anions.[22−24] Here size-selected water cluster anions have been used as embryonic model systems in the hope that the mechanism of electron solvation in polar liquids could be understood on the molecular level. At the same time but along a different direction, both experimental and theoretical studies on the hydrated electrons in liquid water have made significant progress in recent years,[28,29] owing to the advent of ultrafast lasers and supercomputers. The combined efforts between quantum mechanical simulation and femtosecond transient absorption and hole-burning experiments have led to a much improved understanding of the electronic structures of the hydrated electrons and the dynamics of electron solvation in water. Different from the results obtained in water cluster and liquid water, the studies on water clathrates have revealed that the trapping sites in this form of water are vacancies in the water frameworks.[27] Therefore, it is important to ascertain the nature of the hydrated electrons formed in the zeolite cavities and the factors that control their formation.

The electrons trapped by sites in zeolites can be generated in three different ways: (1) introduction of strong reducing agents such as alkali metal vapor and NaN_3,[7−16] (2) photolysis of preadsorbed aromatic molecules such as pyrene and anthracene,[18] and (3) radiolysis using high-energy radiation such

* To whom correspondence should be addressed.
† Present address: Engelhard Corporation, 101 Wood Avenue, Iselin, NJ 08830.
⊗ Abstract published in *Advance ACS Abstracts,* March 1, 1997.

S1089-5647(96)02757-5 CCC: $14.00

as fast electrons, γ-ray, X-ray, and far-UV light.[10,17,19,20] The third method is convenient to study electron trapping in zeolites because no interference occurs from the guest chemical species which are present in the other two methods. Using the radiolysis method, together with spectroscopic measurements, detailed information about electron trapping in zeolites could be obtained.[19,20]

Under high-energy radiation the following processes occur in zeolites:

$$Z \xrightarrow{\beta} h^+ + e^- \quad \text{(ionization of zeolite framework)} \quad (1)$$

$$h^+ \rightarrow h^{\bullet +}_{trap} \quad \text{(hole trapping)} \quad (2)$$

$$h^+ + e^- \rightarrow \text{recombine} \quad \text{(electron−hole recombination)} \quad (3)$$

$$e^- \rightarrow e^-_{trap} \quad \text{(electron trapping)} \quad (4)$$

$$h^{\bullet +}_{trap} + e^-_{trap} \rightarrow \text{recombine} \quad \text{(trapped charge recombination)} \quad (5)$$

$$e^-_{trap} + Q \rightarrow Q^{\bullet -} \quad \text{(quenching of trapped electrons)} \quad (6)$$

Processes 2 and 4 can be expanded further into hole trapping and electron trapping by different species.

$$h^+ \rightarrow Z^{\bullet +} \quad \text{(hole trapping by zeolite framework)} \quad (7)$$

$$h^+ + S \rightarrow S^{\bullet +} \quad \text{(hole scavenging)} \quad (8)$$

$$e^- + Na_n^{n+} \rightarrow Na_n^{(n-1)+} \quad \text{(electron trapping by cation clusters)} \quad (9)$$

$$e^- + (H_2O)_n \rightarrow (H_2O)_n^- \quad \text{(formation of hydrated electrons)} \quad (10)$$

$$e^- + Q \rightarrow Q^{\bullet -} \quad \text{(electron scavenging)} \quad (11)$$

where Z denotes the zeolite framework, $Z^{\bullet +}$ the trapped hole in the zeolite framework, e^- a thermalized electron, and e^-_{trap} the trapped electron. Na_n^{n+} denotes cation clusters that are capable of trapping electrons. S and Q are hole and electron scavengers, respectively, including foreign species such as metal ions introduced by ion exchange, organic molecules adsorbed in the supercage, and defect sites in the zeolites.

Previously, we have investigated most of the above processes related to electron trapping in detail,[20] and Trifunac et al. have studied trapping of positively charged holes in form of oxidation of organic adsorbates in dry zeolites using the EPR technique.[21] In the present study, we report the results of a study of electron and hole trapping by water in zeolites NaX and NaY. The study aims at questions such as the following: (1) What is the nature of the hydrated electrons formed in the zeolite cavities? (2) What is the minimum water content for electron solvation in zeolites? (3) How do water molecules in zeolites affect the cation cluster trapping sites? (4) How is the reactivity of the positively charged holes in hydrated zeolites, i.e., the effect of water on the mechanism of oxidation reactions, in comparison with dry systems?

Experimental Section

Sample Preparation. Zeolites NaX and NaY with Si/Al ratios of 1.4, and 2.5, respectively, were purchased from Aldrich. NaX (Si/Al =1.0) was prepared by following Kühl's procedures[30] with some modifications and then followed by conventional ion exchange with an aqueous solution of NaCl. The zeolites used were examined using the powder X-ray diffractometry and confirmed to be of good quality. Pyrene is adsorbed from a pentane solution into zeolites which have been dried overnight in a 500 °C oven. Methyl viologen divalent cation (MV^{2+}) is quantitatively introduced into zeolites via ion exchange. Benzene is adsorbed in situ by zeolite disc samples from the vapor phase through a high-vacuum line.

Time-Resolved Transient Absorption Measurements. High-energy irradiation of zeolites is performed in a high-vacuum chamber using a 2 ns pulse of fast electron beam from a Febetron 706. A detailed experimental setup for transient absorption measurements has been given in our previous studies.[20] Self-supported discs, similar to those used for FT-IR studies (~10 mg/cm^2), of the zeolite samples are used in diffuse transmittance measurements. The water content of zeolite samples inside the irradiation chamber under different vacuum conditions is estimated from separate experiments using a gravimetric method.

Results and Discussion

Before giving the results, it is pertinent to briefly describe the structures of zeolites used in this study. Zeolites X and Y, structurally similar to the natural mineral faujasite, are synthetic crystalline microporous aluminosilicates, and their frameworks are composed of SiO_4 and AlO_4 tetrahedra. The structures of the zeolites can be considered to be built up of sodalite cages connected through double six-membered rings in a manner of tetrahedron.[31] By this kind of connection, a supercage having a size of 13 Å in diameter with four tetrahedrally arranged entry apertures of size ~7.4 Å is formed in its structure.[30] Due to the presence of AlO_4^{5-} tetrahedra in the zeolite frameworks, negative charges are introduced and require cations such as Na^+ for the charge balancing.

On hydration of zeolites, water molecules occupy both the small (sodalite cage) and large (supercage) cages and can be removed reversibly by evacuation in vacuum and by heating to high temperatures. In fully hydrated zeolites X and Y (equilibrated under water vapor), water fills the supercage and forms a tetrahedrally connected cluster network. The water in zeolite cavities can be arbitrarily divided into four categories: (1) "Free" water in the supercage channel structure from capillary condensation, which is not strongly held by either Na^+ cation or framework. This type of water is very mobile and easily removed by vacuum at room temperature. As we will see later, it plays an important role in the solvation of excess electrons. (2) Coordination water that is coupled to the charge-balancing cations and framework oxygen atoms. This category of water is less mobile and not easily removed by simple vacuum pumping at room temperature but can be removed by thermal desorption at high temperatures. (3) Intermediate water that lies in between the coordination water and the free water. (4) Structured water. An example of this latter type of water is the pentagonal dodecahedron water found in the α-cage of zeolite A.[32]

1. Electron Trapping by Water in Zeolite Cavities. Our previous studies have shown that the water in the hydrated zeolites NaX (Si/Al = 1.4) and NaY (Si/Al = 2.5) traps excess electrons produced by high-energy irradiation of the zeolite frameworks (see eqs 1 and 10).[20] The radiolysis gives rise to the absorption band of hydrated electrons with a maximum spectral position around 720−740 nm. The formation of hydrated electrons (denoted as e_s^- to distinguish it from e_{aq}^- in bulk water) in the zeolites X and Y has been identified by their absorption spectra, their short lifetimes distinct from the long-

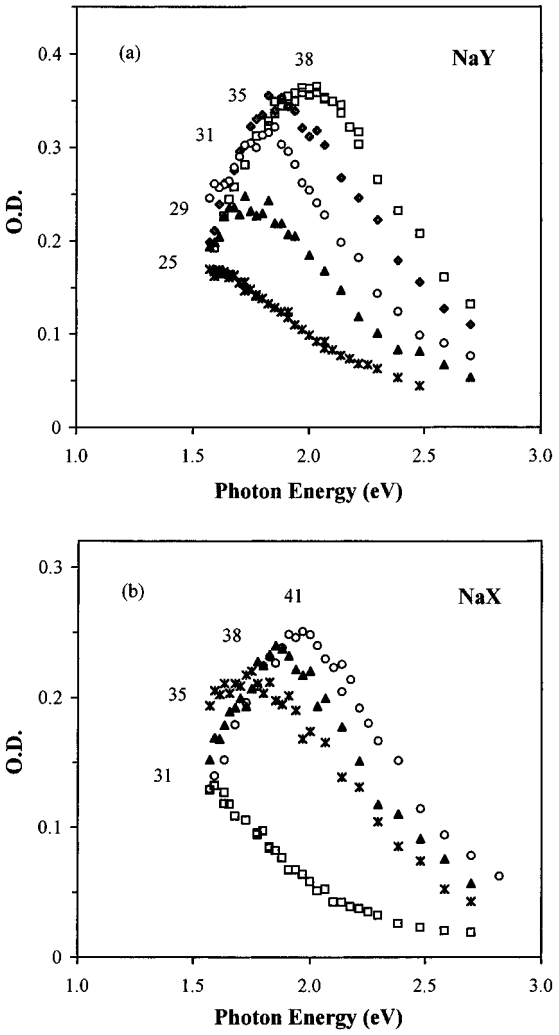

Figure 1. Transient absorption spectra of hydrated zeolites (a) NaY-(2.5) and (b) NaX(1.4) recorded at 20 ns after the electron pulse The water contents are denoted by the number of water molecules per pseudocell (a sodalite cage plus a supercage).

lived cation cluster trapped electrons, and their reactivity toward the typical hydrated electron quenchers such as MV^{2+}. It is found that the hydrated electrons are exclusively located in the supercages and can be quenched completely by gas scavengers such as O_2 and N_2O, provided that the free space is available in the supercage to allow the gas molecules to penetrate into the sample.[20] The results given below provide more detailed information about the nature of electron solvation in zeolite-confined water clusters.

Figure 1 shows the transient absorption spectra of hydrated zeolites Y(2.5) and X(1.4) recorded at ~20 ns after the electron pulse. For each of the zeolite samples, a series of spectra are measured upon removal of water by vacuum pumping. The spectral scan starts with zeolite samples equilibrated under 12 mbar of water vapor where the supercage is completely filled with water. For convenience, the number of water molecules in a pseudo unit cell (a sodalite cage plus a supercage) will be used to denote the water content in a zeolite sample, which is 38 for zeolite Y and 41 for zeolite X, as illustrated in the figure. The spectra of 38 H_2O hydrated NaY and 41 H_2O hydrated NaX (i.e., at the highest water contents) exhibit nearly the same absorption peak around 2.0 eV with a full width of ~0.8 eV at half-maximum. On successive removal of water from the zeolites, a gradual spectral shift toward the longer wavelengths (i.e., lower transition energies) is observed, which is accompanied by a reduction in the intensity of the absorption bands, paralleling the decrease of the water content (Figure 1). Further measurements in the near-IR region is limited by the response of the photomultiplier and the monochromator. The half-bandwidths at the high-energy wing are around 0.5 eV and correspond for all the spectra in zeolites X and Y. No spectral broadening is observed, indicating that the water clusters have a uniform size in zeolites at different water contents. It appears that the previously reported absorption spectra with maxima at 720 nm for NaY and at 740 nm for NaX are only two specific examples among the above spectral series taken under the vacuum conditions used in our earlier work.[20]

The extinction coefficient of the water cluster solvated electrons $\epsilon(e_s^-)$ is measured by a comparison method where the quantitative reaction between e_s^- and MV^{2+} relates $\epsilon(e_s^-)$ to the known extinction coefficient of its product $MV^{\bullet+}$. Specifically, the dynamic quenching of e_s^- (monitored at 620 nm) by MV^{2+} and the simultaneous formation of $MV^{\bullet+}$ (monitored at 390 nm) are measured in a 3.2 mM MV^{2+}-exchanged zeolite NaY. The extinction coefficient of the water cluster trapped electrons in NaY is determined, from the one-to-one correspondence, to be 1.96 x 10^4 M^{-1} cm^{-1} at λ_{max} = 620 nm, using $\epsilon(MV^{\bullet+}) = 4.2 \times 10^4$ M^{-1} cm^{-1} at 390 nm in aqueous solutions.[33] Using the above extinction coefficient for e_s^- in zeolite NaY under 12 mbar of water vapor, the G value of e_s^- is then calculated to be $G(e_s^-) = 5.8$. The dosage absorbed by NaY samples is measured by using $G(e_{aq}^-) = 3.0$ in water (on a nanosecond time scale) as the standard. The present study shows that the hydrated electrons in zeolites exhibits a blue-shifted spectrum at the highest water content. Based on the spectral shape and the extinction coefficient of e_s^- in zeolites, the oscillator strength of the corresponding electronic transition is very close to that of e_{aq}^- in liquid water, i.e., $f = 0.75$. The nearly constant value of f with respect to the water cluster size[24] indicates that the lowering of band intensity with the decreasing water content is due to a decrease in the trapping sites available for the formation of e_s^- in the zeolite supercages.

The spectral red shift with the decreasing water content in zeolites exhibits some similarity with the water cluster anions in the gas phase. Recent experimental studies by Johnson et al. show that the absorption spectra of size-selected water cluster anions $(H_2O)_n^-$ shift to the red (lower energy) as the size of the clusters decreases from $n = 30$ to $n = 18$, 6, and 2.[24] Delocalization of solvated electrons in small water clusters has been clearly shown by a spectral moment analysis.[24] When the cluster size is reduced to $n < 15$, the density distribution of an excess electron trapped by a water cluster spreads significantly outside the boundary of the water cluster itself. The same size effect on electron solvation in water clusters has also been observed in a series of photoelectron detachment experiments by Bowen and co-workers.[23] All these gas phase experimental studies of electron solvation in size selected water clusters have finally established the linkage between $(H_2O)_n^-$ in the gas phase and e_{aq}^- in liquid water. The well-documented hydrated electrons e_{aq}^- in aqueous solutions is just a limiting example of water cluster anions $(H_2O)_n^-$ when the number of water molecules n is large. It tends to support the cavity model proposed early by Ogg,[34] which was further developed by Jortner,[35] and has been recently detailed by Rossky[36] and Landman.[23,37] It is shown that the increasing size of water clusters results in a better solvation of excess electrons, which is characterized by the augmentation of the adiabatic electron binding energy, i.e., the deepening of the electron-trapping depth. The characteristic broad optical absorption around 700 nm exhibited by water cluster solvated electrons is attributed

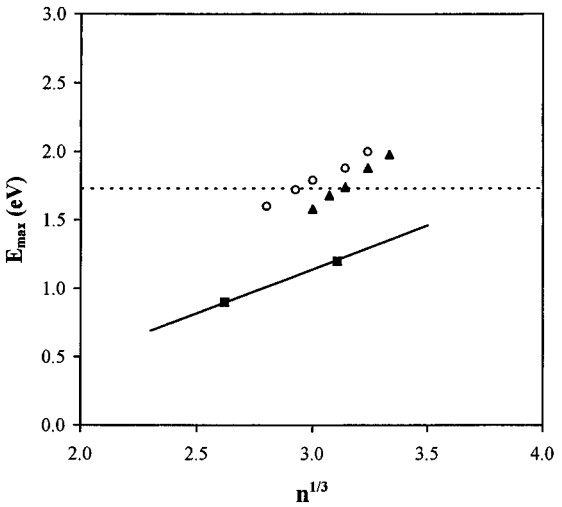

Figure 2. Plot of the maximum position of the absorption band (E_{max}) as a function of the size of water clusters ($r \propto n^{1/3}$) in zeolites X and Y. n is the number of water molecules per supercage. Circles, NaY data; triangles, NaX data; squares with a solid line, the gas phase results by Johnson.[24] The asymptotic value of $E_{max} = 1.73$ eV for very large water clusters is shown as a dashed line.

to the electronic transition from a s-like ground state to three nondegenerate p-like excited states.[36,38] Both experimental and theoretical studies show that the size dependence of the electronic transition results from the variation of electron solvation in small water clusters $(H_2O)_n$ with $n < 100$.[24,38] A detailed quantitative agreement between experiments and theories is yet to be achieved with regard to the critical size of water clusters where the structure of solvated electrons changes from interior bound states to surface bound states.[37,38]

By comparison of what we have observed in hydrated zeolites with the gas phase results, it is confirmed that the water in the cage structures of zeolites differs from the bulk liquid; i.e., it exists in the form of clusters. The red shift of the transient absorption spectra of the water cluster trapped electrons in the zeolite supercage is a consequence of the decrease in cluster size upon dehydration. This parallels that observed for $(H_2O)_n^-$ in the gas phase. The similarity in the spectral shape and the oscillator strength among water cluster trapped electrons in zeolites, e_{aq}^- in the liquid water, and $(H_2O)_n^-$ in the gas phase, is indicative of the same origin of the involved electronic transition in the absorption spectra. However, significant differences exist between $(H_2O)_n^-$ in zeolites and $(H_2O)_n^-$ in the gas phase. Figure 2 shows the variation of the absorption maximum E_{max} (in electronvolts) with the water content in the supercage of zeolites, in comparison with the results from the gas phase studies. The number of water molecules in the supercage of zeolite X and Y, i.e., n is estimated by assuming that each sodalite cage takes four H_2O.[39] The cluster anions $(H_2O)_n^-$, with n changing from 37 to 21 in zeolites, exhibit systematically higher transition energies E_{max} than their counterparts in the gas phase. The difference between the two sets of data is around 0.5 eV. In addition, $(H_2O)_n^-$ in zeolites shows a larger red shift with the decreasing number of water molecules. The effects of the specific structure features of zeolites on the solvation and spectroscopic properties of water cluster trapped electrons are discussed in the following.

Salt Effect. $(H_2O)_n^-$ in zeolites suffers severe electrostatic perturbation by the charge-balancing cations and the negatively charged framework. The spectra of hydrated electrons in the fully hydrated zeolites are blue-shifted by about 0.28 eV relative to that of the hydrated electrons in pure water.[25] Such a blue shift of the hydrated electron spectrum is not unusual and has been observed in micelles[40,41] and in aqueous solutions containing high concentrations of salts.[42] The phenomenon was designated as a "salt effect".[25,42] The spectral blue shift observed in the hydrated zeolites can be interpreted in a similar way. For zeolites X(1.4) and Y(2.5), a simple estimation of the concentrations of Na^+, using their chemical compositions and unit cell volumes, gives comparable Na^+ concentrations to those in solution and micelles, ~8.5 mol/L for the zeolite X and ~6 mol/L for the zeolite Y. It is found experimentally that an inhomogeneous distribution of cations among the different types of cages may occur, and this might result in a deviation from the estimated concentrations.[43,44] X-ray crystallographic studies of zeolites have shown that the migration of Na^+ from the small sodalite cage to the large supercage takes place on hydration and that the reverse occurs on dehydration.[44] As a result, complete hydration may preferentially locate the Na^+ cations in the large supercages. This is due to the stronger interaction of Na^+ with water compared to that with the zeolite framework. Take zeolite NaX as an example, at the highest water content (41 H_2O in a pseudocell), 7−8 of the 10 Na^+ cations are located in the supercage, and the H_2O to Na^+ ratio is around 5. The coordination number of water for each Na^+ cation could be as low as ~4, if we consider that some of the water molecules in the supercages are used for solvation of the negatively charged framework oxygen. The spectral blue shift at this low limit of water coordination could be ~0.28 eV the same as reported in aqueous solutions.[42]

The migration of cations from the supercage to the sodalite cage might take place upon reduction of the water content, leading to a diminution of the salt effect. However, using the literature data, an estimation of the change in the concentration caused by slight dehydration shows that the change in the concentration of Na^+ in the supercages under this condition is not significant.[44] Further experimental support for this argument is provided by the following thermal desorption studies where a significant cation redistribution is found to occur only at a water content even lower than those given in Figure 1. It is therefore concluded that the approximately constant salt background accounts for ~0.28 eV of the ~0.5 eV systematic blue shift of the spectra of water cluster trapped electrons in zeolites relative to those of the gas phase cluster anions $(H_2O)_n^-$.

Effect of Nearest Water Clusters. Water clusters in the supercages of zeolites are interconnected into a channel structure through a tetrahedral coordination. $(H_2O)_n$ in the four nearest-neighbor supercages surrounding a water cluster trapped electron provide additional electron solvation via a long-range electron−water polarization interaction. Both experimental and theoretical studies show that such a long-range interaction between a localized electron and water molecules in its outer solvation shells is effective up to an extent of 15 Å in radius (i.e., six solvation shells).[24,38] The four nearest-neighbor cages are definitely involved in the electron solvation, and a decrease in the size of the neighboring $(H_2O)_n$ clusters results in less solvation of the excess electron localized in the center supercage.

Framework Effect. A cluster anion $(H_2O)_n^-$ in zeolites sits in the supercage, and the interaction between the electron and the zeolite framework contributes additional solvation energy. In contrast to the gas phase water cluster anions, the water cluster trapped electrons in the zeolite cavities experience a strong electrostatic field exerted by the zeolite framework. Here the zeolite framework surrounding a water cluster trapped electron acts as a polar medium, providing additional solvation energy from electron−zeolite polarization interactions.

A combination of polarization solvation by neighboring water clusters and zeolite framework accounts for the rest of the 0.5

eV blue shift of the spectra of cluster trapped electrons relative to $(H_2O)_n^-$ in the gas phase. The spectral shift data for zeolites X and Y parallel with each other with only slight difference, which could be attributed to their similarity in the water cluster size, the salt background, and the framework structure. Compared to Johnson's data and spectral momentum analysis,[24] electrons attached to zeolite confined water clusters exist in interior solvated states with average radii $\langle R^2\rangle^{1/2} < 2.5$ Å. There is no indication of surface solvated states for water cluster trapped electrons $(H_2O)_n^-$ with n reduced to as low as 21, presumably due to the Na^+ perturbation and the extra solvation provided by the neighboring water clusters and the zeolite framework.

The above results obtained in the zeolite systems are directly comparable to those for the gas phase water cluster anions, which clearly show the confinement of the zeolite cavities on the adsorbed water. As far as we know, this is the first report of the size effect on electron localization in molecular clusters in the condensed phase.

2. Migration of Water Cluster Trapped Electrons. The quenching studies[20] of water cluster trapped electrons using electron scavengers such as methyl viologen (MV^{2+}) provide evidence that the water cluster trapped electrons in zeolites are mobile. The mobility of the water cluster trapped electrons changes with the water content. As the water content decreases in zeolites X and Y, the mobility of the water cluster trapped electrons drops. A comparison of the quenching rate constants of the water cluster trapped electrons by MV^{2+} for the samples NaY(2.5) with different water contents gives a quantitative measure of the mobility change. Figure 3a shows the decay traces of the water cluster trapped electrons in the zeolite Y under 12 mbar of H_2O vapor (38 water molecules), monitored at 620 nm, as a function of MV^{2+}. The long-lived part of the decay curve is due to reduced $MV^{\bullet+}$ owing to the spectral overlap in this region. Figure 3b gives the plots of decay rates (obtained by computer curve fitting) of water cluster trapped electrons in the 38 and 31 water molecule hydrated zeolites Y against the concentration of MV^{2+}. From Figure 3b, the quenching rate constants under these two water contents were obtained: 1.26×10^8 M^{-1} s^{-1} for the 31 water molecule hydrated sample and 3.55×10^8 M^{-1} s^{-1} for the fully hydrated sample. Due to its size and charge, the mobility of MV^{2+} in the cavities could be neglected, and the diffusion coefficients of the water cluster trapped electrons (D_e) in NaY with different water content is estimated using the Smoluchowski relation[45]

$$k = 4\pi NRD_e \qquad (12)$$

where N is the Avogadro constant and R is the effective reaction radius which includes the electrostatic interaction between MV^{2+} and water cluster trapped electron. With the reaction radius R taken as 16 Å on the basis of the rate constant measured in aqueous solution,[33] $k = 7.5 \times 10^8$ M^{-1} s^{-1}, the values of D_e estimated for these two samples are 1.2×10^{-7} cm^2 s^{-1} for the 31 water molecule hydrated sample and 3.5×10^{-7} cm^2 s^{-1} for the 38 H_2O hydrated sample. A comparison of the values shows that complete hydration increases the mobility of water cluster trapped electrons by 3-fold compared to that with 31 water molecule per pseudocell.

The dependence of the reactivity of water cluster trapped electrons on the water content is also evident from the systematic variation of the lifetime of $(H_2O)_n^-$ in blank zeolites free from guest molecules. As will be shown later, the decay of $(H_2O)_n^-$ in the absence of quenchers is due to its reactions with hydroxyl radicals $OH^\bullet$ and H^+ which are derived from the oxidation of water by the positively charged holes. The gradual increase of the $(H_2O)_n^-$ lifetime from 0.2−0.4 to 3−4 μs upon evacuation of water up to ∼24 H_2O molecules per supercage results from a slowing down of the movement of all the reactive species involved in the diffusion-limited reactions, such as $OH^\bullet$ + $(H_2O)_n^-$ and H^+ + $(H_2O)_n^-$.

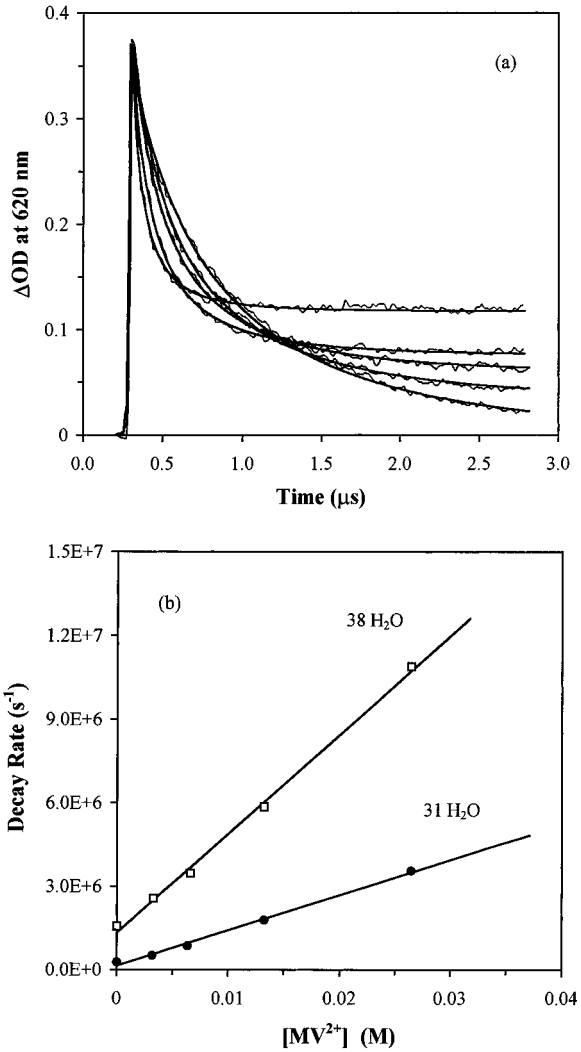

Figure 3. (a) Decay curves of the water cluster trapped electrons, monitored at 620 nm, as a function of MV^{2+} concentration in 38 H_2O hydrated NaY. The smooth lines give the fittings by a Gaussian kinetics. (b) Plots of average decay rates of water cluster trapped electrons under different hydration conditions against the concentration of MV^{2+}. Squares, 38 H_2O hydrated NaY; dots, 31 H_2O hydrated NaY. The straight lines are the linear regression of the rate data.

Even though the diffusivity of water cluster trapped electrons increases with increasing water content in the zeolite, it is still at least 2 orders of magnitude slower than that of hydrated electrons in liquid water,[46] $D_e = 4.9 \times 10^{-5}$ cm^2 s^{-1}. It is interesting to point out that the transport of e_{aq}^- is quite different from that of a classical anion in the sense that it cannot be described by a hydrodynamic model in a dielectric continuum. Previous experimental studies found that the movement of e_{aq}^- is markedly faster than a simple anion in aqueous solutions and exhibits a higher activation energy.[46,47] Recent quantum dynamics simulations found that a high local fluctuation of the orientation of water molecules surrounding an excess electron and the essentially instantaneous adiabatic response of the electron wave function to the change in water configuration lead to a high mobility of electrons relative to classical ions such as Br^-.[48] The diffusivity of e_{aq}^- is shown to closely follow the self-diffusion of water. The enhanced transport of e_{aq}^- in liquid water can be well understood within the framework of such an

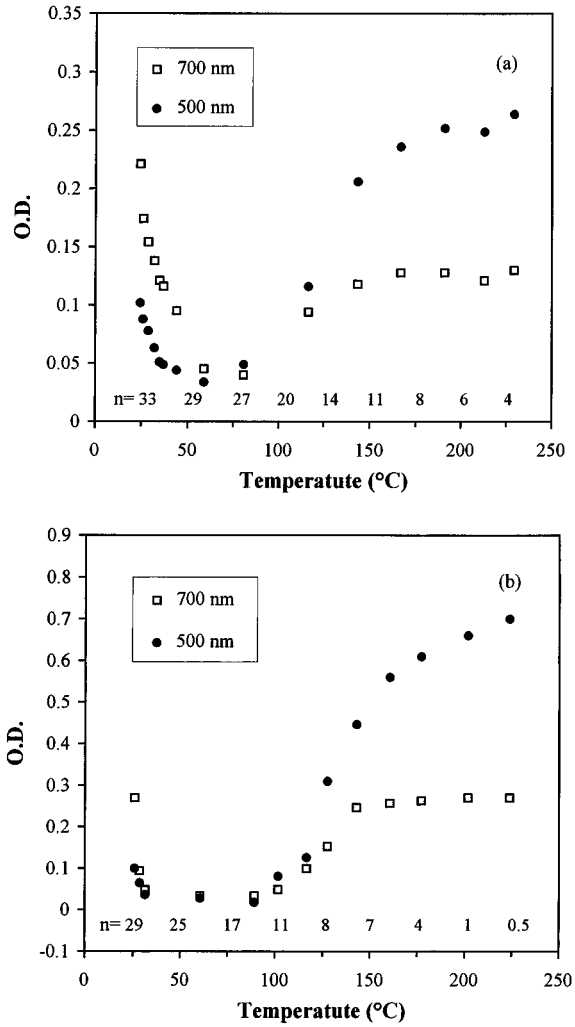

Figure 4. Changes of band intensities monitored at 500 and 700 nm on heating the zeolites (a) NaX(1.4) and (b) NaY(2.5) under a vacuum of 5×10^{-2} Torr. The numbers are the corresponding water content per pseudocell.

adiabatic model,[48,49] without invoking the long held quantum mechanical tunneling mechanism.[50] For water cluster trapped electrons in zeolites, the above adiabatic transport of electrons is restricted by the nanometer cage structure. On the one hand, the interactions of water with the Na^+ cations and the inner surface of the supercage lead to a nearly 10 times decrease in the water mobility in zeolites relative to that in liquid water, as demonstrated by the results of NMR measurements.[51] On the other hand, the window between two neighboring supercages with a diameter of 7.4 Å provides an energetic barrier for the electron migration from one supercage to the neighboring supercages. The size effect on the solvation energetics indicates that an excess electron localized at the window site sits in an unfavorably higher energy state than that solvated in the 13 Å wide supercage. The adiabatic motion of electron is thus modulated by a bottleneck effect in the sense that large fluctuation of water molecules in the solvation shells is needed for an electron to adiabatically reach a higher energy state and pass through the window. The drop of the water mobility in zeolite cages, which does not favor the large-amplitude fluctuation, might explain the 2 orders of magnitude difference in electron mobility between bulk water and topologically continuous water channels confined by the zeolite framework. With decreasing amounts of water in zeolites, less bridging water is available at the window, which makes the electron passage through the window even more difficult.

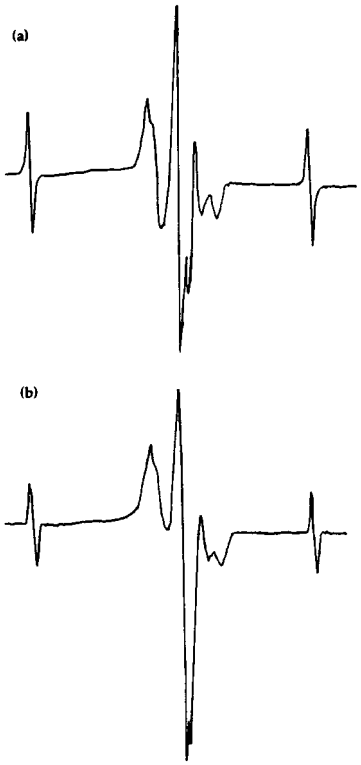

Figure 5. EPR spectra of (a) 29 water molecule hydrated zeolite NaY-(2.5) and (b) 17 water molecule hydrated zeolite NaY(2.5) after γ-irradiation for 20 min at 77 K.

3. Formation of Cation Clusters on Dehydration. Figure 4 shows the changes of the band intensity monitored at 500 and 700 nm on heating the zeolite samples under a vacuum of 5×10^{-2} Torr. The corresponding water content at these temperatures is also given. At room temperature, the absorption signals monitored at 500 and 700 nm are all due to water cluster trapped electrons (broad absorption band). When the temperature is raised, the intensities of these absorptions decrease. At temperatures above 90 °C, the absorptions are no longer due to the water cluster trapped electrons but rather to the cation cluster trapped electrons.[18,19] The signal at 500 nm originates from Na_4^{3+}, while that at 700 nm is due to Na_3^{2+}.[18,19] Within the temperature range of 40−90 °C, the absorptions become very weak at both wavelengths (see Figure 4). The change of the spectra with increasing temperature (decreasing water content) indicates that there are none or very few cation cluster electron trapping sites if the number of water molecules is above 17 in the zeolite Y and 27 in the zeolite X and that these trapping sites are formed only when the water molecules are below these levels on removing water. The presence of the weak signal region is due to the spectral red shift out of the spectral window examined and also to the very low concentration of cation cluster trapped electrons. The presence of water cluster trapped electrons in this temperature (water content) range was confirmed by studies using electron paramagnetic resonance spectroscopy. Figure 5 shows the EPR spectra of 29 H_2O hydrated and 17 H_2O hydrated zeolites Y taken at 77 K after γ-irradiation. On the basis of the literature, the central signal with $g = 2.0036$ is known to be due to the water cluster trapped electrons,[52] while the rather broad signals with a fine structure are to the trapped positively charged holes. The sharp signals on both side of the central signals with hyperfine coupling $a =$ 508 G are due to atomic hydrogen.[53] The presence of atomic hydrogen may result from decomposition of the hydroxyl groups present in the zeolites, as seen in the case of silica,[54] and from the secondary reactions of hydrated electrons with H^+.[55] From

the EPR spectra, it is clear that only the water cluster trapped electrons are present in the sample containing 17 water molecules. There is no indication of cation cluster trapped electrons. The spectral similarity between the high and low water content samples confirms that the water cluster trapped electrons are still present in this sample, even though the transient absorption spectra show very weak absorptions in the spectral region examined. The results shown above lead to the conclusion that (1) no cation cluster trapping sites are present when the water content is above 17 and 27 water molecules per pseudocell in zeolites Y(2.5) and X(1.4), respectively, (2) water adsorbed in the zeolites tends to "destroy" the cation cluster trapping sites reversibly, and (3) the cation cluster trapping sites are only formed during dehydration. This picture of the formation of cation cluster trapping sites is in agreement with the redistribution of cations from the cage void to the framework wall sites and from the large cage to the small cage observed on removal of water. It is more clearly shown by the following studies on the zeolite NaX with the lowest Si/Al ratio.

Due to its low Si/Al ratio, zeolite X(1.0) has a higher Na^+ content than the zeolite X(1.4). The increase in Na^+ content increases the possibility of forming cation clusters capable of trapping electrons, and because of this, it may be possible to observe the coexistence of cation cluster trapped electrons and water cluster trapped electrons at relatively higher water content. Figure 6a shows the transient absorption spectra of water vapor saturated (41 water molecules per pseudocell) and 31 water molecule hydrated zeolite NaX(1.0) recorded at 20 ns after the electron pulse. For the fully hydrated zeolite, only one band with a maximum at ~600 nm is observed, which is similar to that seen for the fully hydrated zeolites X(1.4) and Y(2.5), while for the 31 water molecule hydrated zeolite X(1.0), two bands at ~540 and ~750 nm are seen. These two bands originate from cation cluster trapped electrons, Na_4^{3+}, and water cluster trapped electrons, $(H_2O)_n^-$, respectively. The presence of both types of trapped electrons indicates that the increase in Na^+ content indeed facilitates the formation of cation cluster electron trapping sites. The variation in intensities of the signals monitored at 700 and 550 nm as a function of water content is shown in Figure 6b. It is similar to that seen for the zeolites X and Y (Figure 4). The transition from electron solvation by water clusters to electron localization by cation clusters occurs at a hydration level of 31−34 water molecules. In comparison with the zeolites X(1.4) and Y(2.5), it is obvious that cation cluster electron trapping sites can form at relatively higher water content in the zeolites with lower Si/Al ratios.

Figure 7a illustrates the time-resolved traces of Na_4^{3+} (monitored at $\lambda = 550$ nm) and $(H_2O)_n^-$ ($\lambda = 750$ nm) in 31 water molecule hydrated NaX(1.0). Cation cluster trapped electrons Na_4^{3+} exhibit an instantaneous formation followed by a buildup over ~2 μs. The static component indicates that the cation clusters capture thermalized electrons in less than 20 ns, while the dynamic growth with the simultaneous decay of hydrated electrons on the same time scale suggests that electron transfer from $(H_2O)_n^-$ to the cation cluster sites takes place. The signal monitored at 550 nm is fitted to a biexponential function including both growth and decay terms.

$$A(t) = (A_f + A_p)\exp(-k_d t) - A_f \exp(-k_f t) \qquad (13)$$

Information is then obtained about the cation cluster formation rate, k_f, and the yield, A_f, due to the electron transfer, and the cation cluster decay rate, k_d, and the yield of the statically formed cation cluster trapped electrons, A_p. Meanwhile, the signal at 750 nm is fitted to a biexponential decay function with the slow component attributed to the overlapping signal from Na_4^{3+}. The

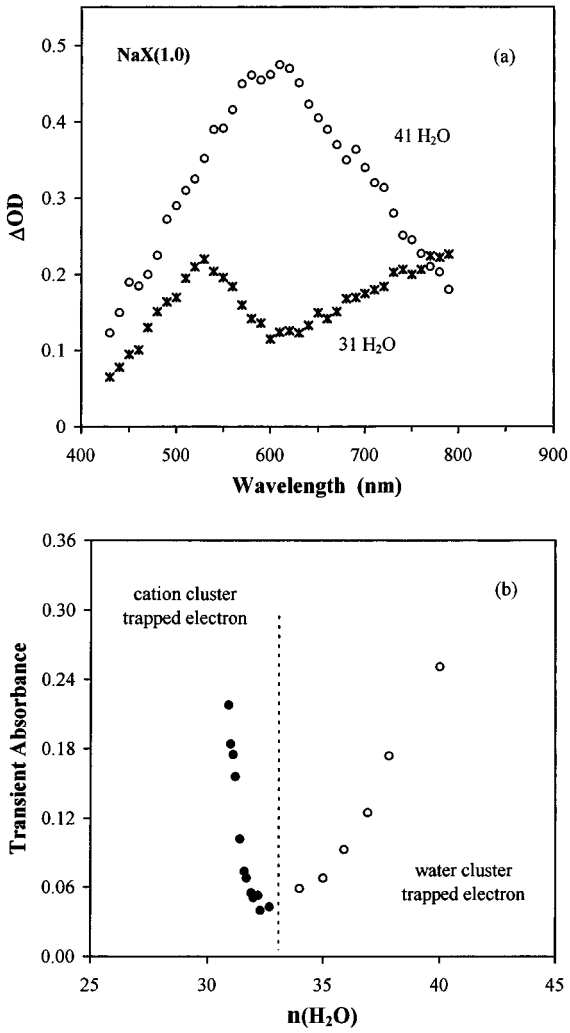

Figure 6. (a) Transient absorption spectra of 41 water molecule hydrated and 31 water molecule hydrated zeolite NaX(1.0) recorded at 20 ns after the electron pulse. (b) Variation in intensity of the signals measured at 550 nm (dots) and 700 nm (open circles) as a function of the water content in zeolite NaX(1.0).

following rates are obtained from a nonlinear least-squares fitting procedure: 1.30×10^6 s^{-1} for the growth of the cation cluster trapped electrons, 2.6×10^4 s^{-1} for the decay of Na_4^{3+}, and 1.24×10^6 s^{-1} for the decay of $(H_2O)_n^-$. The close match between the decay rate of $(H_2O)_n^-$ and the growth of Na_4^{3+} shows that electrons are transferred from the water clusters to the cation cluster trapping sites. From this observation, it is concluded that the cation clusters such as Na_4^{4+} are stronger electron trapping sites than the water cluster sites and that electron transfer between these two kinds of sites takes place once cation cluster trapping sites are formed from dehydration.

$$(H_2O)_n^- + Na_4^{4+} \rightarrow (H_2O)_n + Na_4^{3+} \qquad (14)$$

The formation of cation cluster trapped electrons in NaX-(1.0) with different water contents is monitored at 550 nm (Figure 7b). These decay traces are analyzed using eq 13. The variation of the kinetic parameters as a function of water content is plotted in Figure 7c,d. As the water content decreases, the formation rate, k_f, of cation cluster trapped electrons, from electron transfer reaction 14, increases, indicating that the electron transfer rate increases as the water clusters become smaller. In contrast, the decay rate, k_d, of the cation cluster trapped electrons formed decreases, implying that the cation cluster trapped electrons become more stable as the water

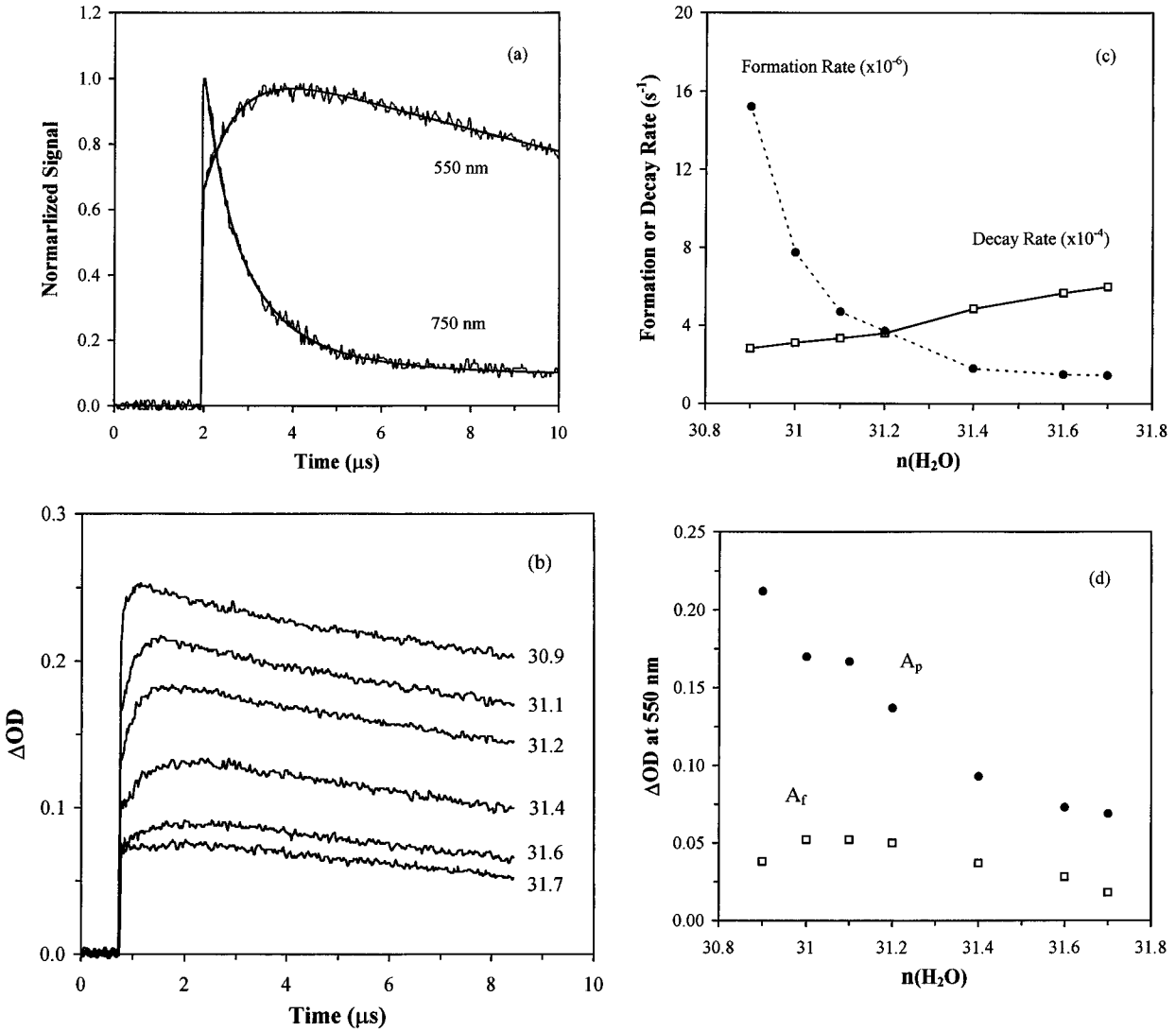

Figure 7. (a) Decay traces monitored at 550 and 750 nm in NaX(1.0) with 30.5 H_2O per pseudocell. Smooth lines show the biexponential fitting curves (see text). (b) The transient signals monitored at 550 nm in NaX(1.0) at different water contents as denoted by the number of water molecules per pseudocell. (c) Variation of the formation rate k_f and the decay rate k_d of cation cluster trapped electrons with the water content. (d) The yield of cation cluster trapped electrons formed dynamically via electron transfer, A_f, and the yield of the statically formed cation cluster trapped electrons, A_p, as functions of the water content.

content is decreased. The yield of the promptly formed cation cluster trapped electrons continuously increases with decreasing water content, indicating that more cation cluster sites are formed and more excess electrons are captured directly. However, for the cation cluster trapped electrons formed via the electron transfer, the yield first increases with decreasing the water content and then decreases with further removal of water and passes through a maximum at around 31 water molecules. This phenomenon reflects that, with decreasing water content, more water clusters can no longer hold the electrons and have to give their electrons to the cation cluster sites. Further removal of water decreases the number of water clusters, leading to a decrease in the yield of this portion of the cation cluster trapped electrons. The results given above clearly demonstrate that the cation cluster trapping sites are indeed formed during the process of dehydration and that cation cluster trapping sites are stronger electron-accepting sites than the water clusters present in the system. It is worth mentioning that electron transfer could also be observed in the zeolite X(1.4) after prolonged evacuation, but the buildup of absorption signals is not as significant as that seen for the zeolite X(1.0).

It is also seen from Figure 7a−d, that the evolution of the electron transfer process occurs only in a very narrow range of water content. This implies that the significant cation relocation in the system to form cation cluster trapping sites occurs quickly at that water level, and the cation cluster trapping sites, once formed, become dominant for the electron trapping.

4. Reactions of Positively Charged Holes. The above results show that electrons generated by radiolysis of the zeolite frameworks are ejected and subsequently trapped by the water clusters or the Na^+ cation clusters. However, the other half of the story is still missing. This concerns the chemistry derived from the positive holes which are produced in pairs with electrons. For completely dehydrated zeolites, it has been shown that the positively charged holes either are stabilized on the zeolite framework[20] or react with the organic guest molecules to form oxidized products.[21] Trifunac et al. have reported the formation of various cation radicals in radiolysis of zeolites containing organic adsorbates.[21] As far as we know, no work has been done on this aspect in hydrated zeolites. In the following studies, aromatic molecules are introduced in zeolites to probe the possible oxidation reactions.

Pyrene in Zeolite KX. Figure 8a illustrates the transient absorption spectra of pyrene loaded zeolite KX under both dehydrated and hydrated conditions. K^+ cation exchanged zeolite X is used here to give an open spectral window in the

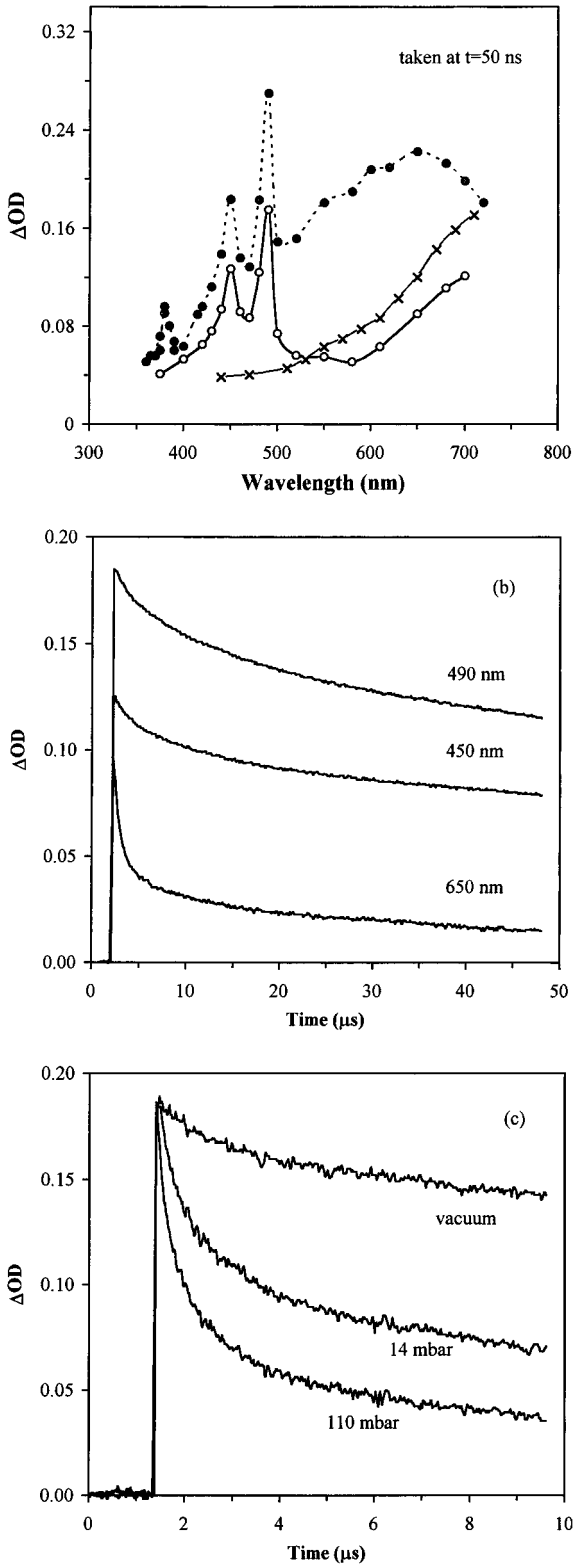

Figure 8. (a) Transient absorption spectra of dehydrated and hydrated zeolite KX. Crosses, blank dehydrated KX; open circles, dehydrated KX loaded with pyrene; dots, hydrated KX with pyrene. The pyrene loading is 2.2×10^{-5} mol/g. (b) Time-resolved traces monitored at 450, 490, and 650 nm in dehydrated Py/KX. (c) Dynamic quenching of the pyrene anion radicals in dehydrated KX by oxygen at different pressures as indicated.

400−500 nm region for the spectroscopic measurements of pyrene transient species. Immediately after irradiation of dehydrated KX sample with a pyrene loading of 2.2×10^{-5} mol/g, two narrow bands centered around 450 and 490 nm are observed, indicative of the instantaneous production of cation radicals and anion radicals of pyrene from reactions of pyrene with energetic holes and excess electrons, respectively.

$$h^+ + Py \rightarrow Py^{\bullet +} \quad (15)$$

$$e^- + Py \rightarrow Py^{\bullet -} \quad (16)$$

A broad absorption above 500 nm is due to the cation cluster trapped electrons, K_3^{2+}. This assignment is based on previous work[56] and the spectrum of K_3^{2+} produced in a blank dehydrated KX sample under the same irradiation conditions (see Figure 8a). The ratio of ~1.5:1 between the $Py^{\bullet -}$ band and that of the $Py^{\bullet +}$ implies that these ions are produced in about equal amounts. Figure 8b shows that both $Py^{\bullet +}$ and $Py^{\bullet -}$ are long-lived with a half-lifetime longer than 100 μs, in contrast to the fast decay of K_3^{2+}. The same nonexponential decay kinetics of $Py^{\bullet +}$ (measured at 450 nm) as that of $Py^{\bullet -}$ (at 490 nm) suggests that charge neutralization might occur within the geminate pyrene cation and anion pairs via electron tunneling, if we consider that minimal movement of pyrene molecules is involved on the microsecond−millisecond time scale. The pyrene anion band is quenched by oxygen in a dynamic fashion (Figure 8c). However, the quenching rate constant $k \sim 2.6 \times 10^4$ Torr^{-1} s^{-1} is significantly lower than that observed in porous alumina,[57] which might result from a partial blocking of the pyrene adsorption sites at high pyrene loadings. Compared to the blank dehydrated KX sample, the intensity of the broad K_3^{2+} band is reduced concomitant with the formation of $Py^{\bullet -}$, indicative of a competitive electron capture by pyrene and cation cluster K_3^{3+}. Even at a high pyrene loading of 6.0×10^{-5} mol/g, only 33% of electrons are scavenged by pyrene due to the inhomogeneous distribution of pyrene inside the zeolite sample. The aggregation of pyrene is revealed by the presence of excimer emission from a separate fluorescence measurement.

Upon equilibrating the dehydrated Py/KX sample under 11 mbar of water vapor, a different transient absorption spectrum is observed. The K_3^{2+} band is replaced by another broad absorption centered at 650 nm, which is assigned to water cluster trapped electrons, $(H_2O)_n^-$. The bands of $Py^{\bullet +}$ and $Py^{\bullet -}$ sit at the high-energy wing of the $(H_2O)_n^-$ spectrum with nearly the same intensities as observed in the dehydrated sample. In addition, a new narrow band appears around 375 nm, which is tentatively assigned to the 1-hydroxylpyrenyl radical ($PyOH^{\bullet}$). This is based on the previously reported spectrum of $PyOH^{\bullet}$ in aqueous solution.[58] The rapid production of $PyOH^{\bullet}$ well within 1 μs could not be understood by the slow hydrolysis of $Py^{\bullet +}$ in water. This suggests that hydroxyl radicals might be the precursor species and that $PyOH^{\bullet}$ is produced via an $OH^{\bullet}$ addition reaction.[58]

$$OH^{\bullet} + Py \rightarrow PyOH^{\bullet} \quad (17)$$

Evacuation of water by vacuum pumping results in a significant decrease of the $PyOH^{\bullet}$ yield. The same phenomenon will be discussed in MV^{2+} loaded zeolite NaY. A possible mechanism for the formation of hydroxyl radicals in hydrated zeolites might be the oxidation of water by the positive holes initially generated in the framework, in analogy to the direct ionization of H_2O molecules in high-energy excitation of water clusters and liquid water.[59,60]

$$h^+ + (H_2O)_n \rightarrow OH^{\bullet} + (H_2O)_{n-1}H^+ \quad (18)$$

The lowering of the ionization potential of water in the liquid phase[61] and the stabilization of the proton H^+ by water and the zeolite framework make reaction 18 energetically favorable.

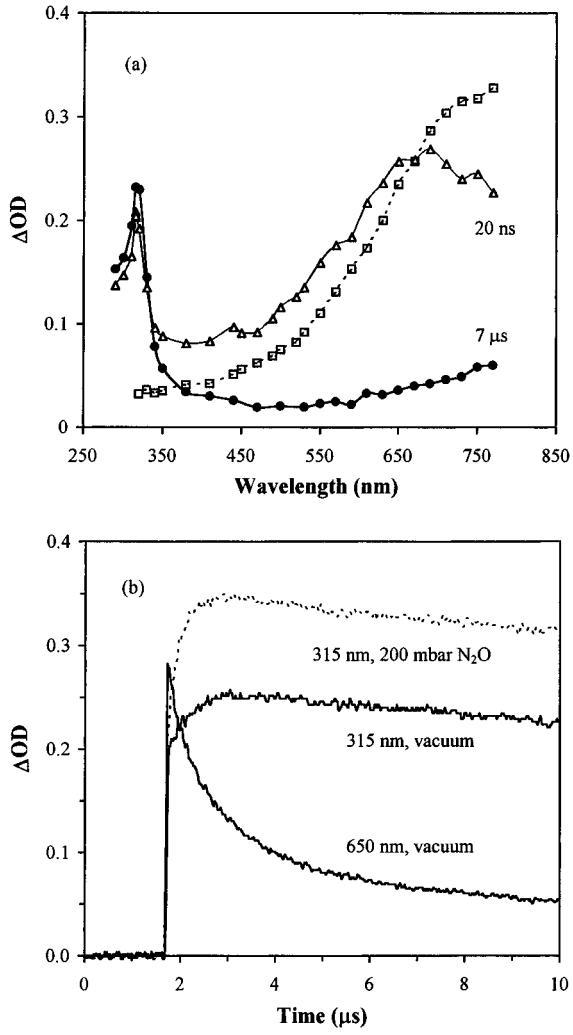

Figure 9. Reaction of benzene in hydrated zeolite Y. (a) Transient absorption spectra of a zeolite disc before and after absorption of benzene from the vapor phase. Squares, blank hydrated NaY under a vacuum of 3×10^{-2} Torr; triangles, after introduction of benzene vapor, spectrum taken at 20 ns; dots, after benzene adsorption, spectrum taken at 7 μs. (b) Signals taken at 315 and 650 nm respectively in vacuum and in the presence of nitrous oxide. The effect of introduction of 200 mbar of N_2O on the 315 nm band is shown as a dashed line.

Quantitative studies of reactions 17 and 18 in zeolite systems are complicated by the heterogeneous distribution of probe molecules and competition between pyrene and water in reactive trapping of the positive holes. Further work is carried out using benzene and methyl viologen as probes for specific examination of the formation and reactivity of hydroxyl radicals. The high ionization potentials of benzene and MV^{2+} do not favor the direct oxidation of organic probes as illustrated in reaction 15.

Formation of Hydroxylcyclohexadienyl Radicals. Figure 9a shows the spectrum of blank hydrated zeolite NaY under a vacuum of 3×10^{-2} Torr and the effect of absorption of benzene vapor. Only water cluster trapped electrons are observed in the blank NaY sample. Absorption of a small amount of benzene on the order of $10^{-5}-10^{-4}$ mol/g gives rise to a new absorption band around 315 nm, with a simultaneous blue shift and a reduction of the $(H_2O)_n^-$ band. Such a blue shift of the $(H_2O)_n^-$ spectrum upon introduction of vapors of hydrocarbons, such as *n*-butane, *n*-pentane, and cyclohexane, is indicative of the structural changes in water clusters. The immiscibility between water and these hydrocarbon compounds might induce reorganization of water clusters within the zeolite system. After the decay of hydrated electrons within 7 μs, only the 315 nm band is observed. The time-resolved measurements at 315 nm clearly show a transient formation over 1−2 μs (Figure 9b). Introduction of 200 mbar of N_2O gas leads to a complete quenching of the water cluster trapped electrons within 20 ns and simultaneously an increased production of the 315 nm band. Here additional hydroxyl radicals are produced from the well-known N_2O reaction with solvated electrons.[60,62]

$$N_2O + (H_2O)_n^- \rightarrow OH^\bullet + OH^- + N_2 + (H_2O)_{n-1} \quad (19)$$

Based on the spectral characteristics and the N_2O effect, the 315 nm band can be assigned to the hydroxylcyclohexadienyl radical, $BOH^\bullet$, derived from the $OH^\bullet$ radical addition to benzene ring.[63]

$$OH^\bullet + \text{benzene} \rightarrow BOH^\bullet \quad (20)$$

The strong signal of the $BOH^\bullet$ radicals manifests the high yield of hydroxyl radicals in radiolysis of hydrated zeolites.

$OH^\bullet$ Addition to Methyl Viologen. The uniform distribution of MV^{2+} exchanged into the zeolite supercages provides a better model system for quantitative measurements of $OH^\bullet$ reaction kinetics. Figure 10a shows the transient spectra of the hydrated zeolite NaY containing 1.0 MV^{2+} per unit cell recorded at 100 ns and 20 μs after the electron pulse, together with their difference spectrum. The spectrum recorded at $t = 100$ ns shows only the two characteristic absorption bands of the reduced methyl viologen $MV^{\bullet+}$ around 390 and 590 nm. As the time evolves, a new band grows in with its maximum at 470 nm, which is more clearly seen from the spectrum taken at $t = 20$ μs. The difference spectrum is in a good agreement with the one reported in aqueous solutions of methyl viologen, which has been assigned to the $OH^\bullet$ adduct of MV^{2+}, $OH-MV^{\bullet 2+}$.[64]

$$OH^\bullet + MV^{2+} \rightarrow OH-MV^{\bullet 2+} \quad (21)$$

The unique presence of the $OH^\bullet$ adduct in the zeolite clearly demonstrates that the positively charged holes generated in radiolysis react with the water in the cavities as described in eq 18, producing a large amount of $OH^\bullet$ radicals as the secondary oxidative species.

The yields of $OH-MV^{\bullet 2+}$ for different MV^{2+} loadings are determined at 40 μs after the electron pulse. The reduced methyl viologen is used as the internal reference, based on the quantitative production of $MV^{\bullet+}$ from its reactions with electrons.[20] The extinction coefficients of $OH-MV^{\bullet 2+}$, $\epsilon_{470\text{ nm}} = 16\,000$ M^{-1} cm^{-1}, and $MV^{\bullet+}$, $\epsilon_{590\text{ nm}} = 14\,000$ M^{-1} cm^{-1}, are taken from the literature.[33,64] The G value of $OH-MV^{\bullet 2+}$ in NaY with 1.0 MV^{2+} per unit cell is $G = 4.7$. Extrapolation of the $1/G \sim 1/[MV^{2+}]$ plot to the high $[MV^{2+}]$ limit gives the G value of $OH^\bullet$ radicals produced in the system, $G_{OH^\bullet} = 6.0$ (Figure 10b). It is thus concluded that (1) the charge separation efficiency is very high in zeolite systems, (2) the positive holes react preferentially with water in the zeolite cavities, and (3) trapping of electrons and holes by water clusters produces equal amounts of hydrated electrons and hydroxyl radicals in fully hydrated zeolites.

Figure 10c gives the time-resolved traces of $OH-MV^{\bullet 2+}$ monitored at 470 nm for the samples containing different amounts of MV^{2+}. The dynamic formation of $OH-MV^{\bullet 2+}$ adduct is clearly seen from the growth of the signals over many microseconds. The kinetics of reaction 21 as revealed from Figure 10c is nonexponential, with a slow growing component more clearly resolved at low MV^{2+} loadings. The growth approaches a single-exponential kinetics at $[MV^{2+}] = 0.106$ M. The initial spikes observed at low concentrations of MV^{2+} are

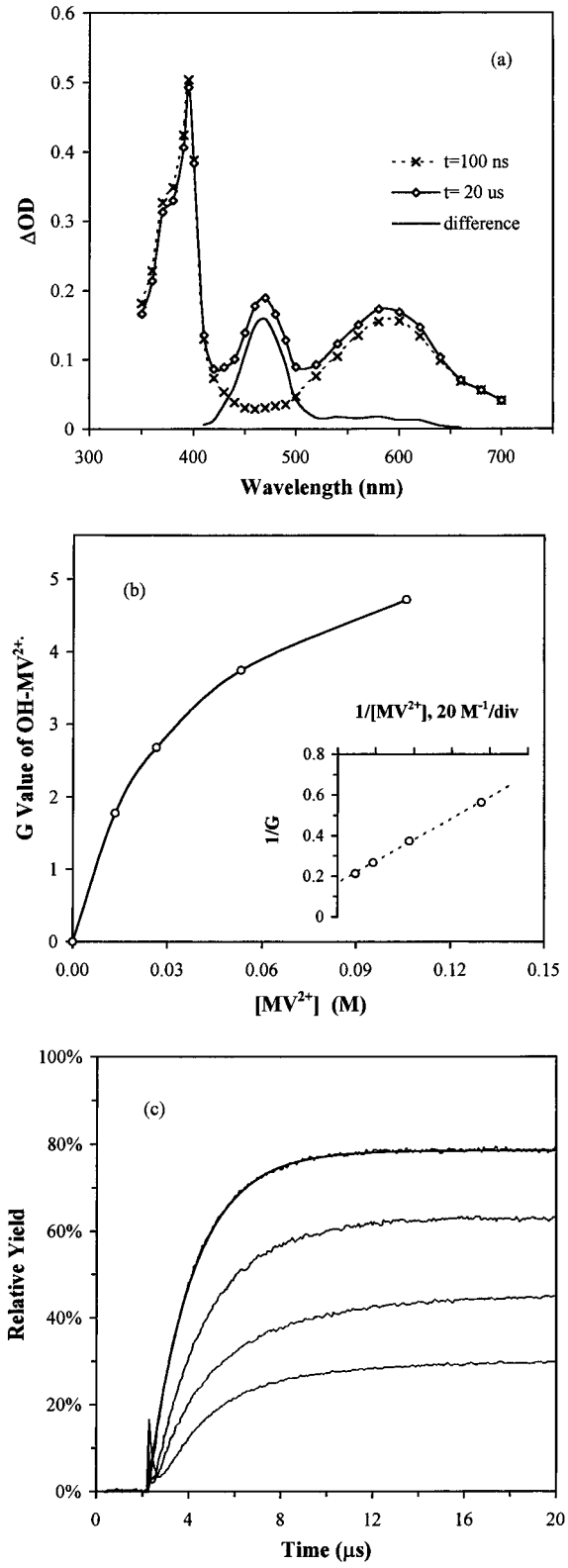

Figure 10. (a) Transient absorption spectra of fully hydrated NaY containing 1.0 MV^{2+}/uc recorded at 100 ns and 20 μs after the electron pulse, with the difference spectrum also shown. (b) Yields of the $OH^{\bullet}$ adduct ($OH-MV^{\bullet 2+}$) as measured in G values at different MV^{2+} loadings. Insert: extrapolation of the $1/G \sim 1/[MV^{2+}]$ plot for the G value of $OH-MV^{\bullet 2+}$ at the high limit of $[MV^{2+}]$. (c) Time-resolved difference signals monitored at 470 nm exhibit nonexponential formation kinetics. $[MV^{2+}] = 0.0125$, 0.0252, 0.053, and 0.106 M from the bottom trace to the top. The long-lived component formed right after the pulse due to $MV^{\bullet +}$ is subtracted to show the dynamic formation of the $OH^{\bullet}$ adduct.

due to the fast decay of the overlapping hydrated electron signals. An analytical description of the kinetics is perplexed

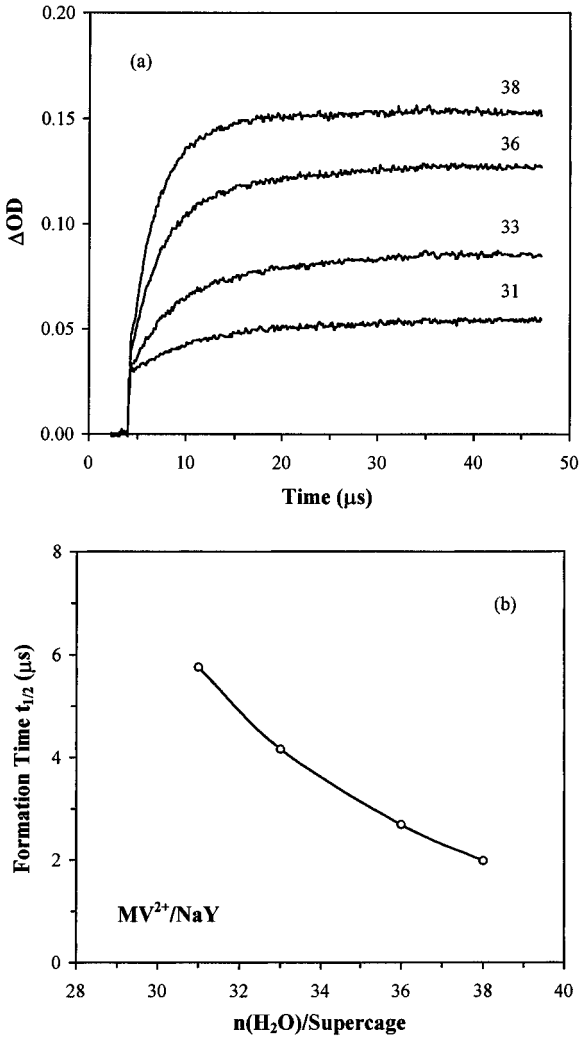

Figure 11. (a) Effect of removal of water by vacuum pumping on the formation of the $OH^{\bullet}$ adduct in NaY. Transient traces are collected at 470 nm with $[MV^{2+}] = 0.053$ M. (b) Variation of the half formation time $t_{1/2}$ with the water content in the zeolite sample MV^{2+}/NaY.

by the restricted movement of $OH^{\bullet}$ in the water channels of hydrated zeolites and the $OH^{\bullet} + OH^{\bullet}$ dimerization reaction due to the nonhomogeneous nature of the radiolytic events. An estimation of the reaction rate is given below using the Stern−Volmer approximation. The kinetic trace of $OH-MV^{\bullet 2+}$ at $[MV^{2+}] = 0.106$ M is fitted to an exponential function with a formation rate of $5.27 \times 10^5\ s^{-1}$. From the 80% yield of $OH-MV^{\bullet 2+}$ at this MV^{2+} concentration, the average rate of the second-order dimerization reaction in competition with reaction 21 is $1.05 \times 10^5\ s^{-1}$. The rate constant of the $OH^{\bullet}$ addition reaction is estimated to be $3.98 \times 10^6\ M^{-1}\ s^{-1}$, which is 2 orders of magnitude lower than that in liquid water.[64] Instead of being activation controlled, the reaction is limited by the slow diffusion of $OH^{\bullet}$ radicals through the zeolite supercages. The diffusion constant of $OH^{\bullet}$ is estimated to be $D = 1.04 \times 10^{-8}\ cm^2/s$ using the Smoluchowski relationship. In comparison with the water cluster trapped electrons, the mobility of $OH^{\bullet}$ radicals is even slower, which may be due to the strong interactions between the dipolar $OH^{\bullet}$ radicals and the zeolite framework.

The diffusivity of $OH^{\bullet}$ radicals is also affected by the water content in the zeolites. Figure 11a shows the changes of the kinetic traces of $OH^{\bullet}$ adduct formation on slight evacuation of water. As shown in Figure 11b, with the removal of water from the sample the half formation time $t_{1/2}$ increases steadily, which corresponds to the decreasing formation rate of the $OH^{\bullet}$ addition reaction, i.e., the slowing down of the diffusive motion of the

$OH^•$ radicals. This phenomenon demonstrates that the movement of $OH^•$ radicals relies on water as a transport medium. The solvation of $OH^•$ by water molecules makes its movement strongly correlated with the collective motion of water in zeolites.

It is worth mentioning that the decay of water cluster trapped electrons in blank hydrated zeolites is due to its reactions with $OH^•$ and H^+, the same as those reported in aqueous solutions.

$$(H_2O)_n^- + OH^• \rightarrow (H_2O)_n + OH^- \quad (22)$$

$$(H_2O)_n^- + H^+ \rightarrow (H_2O)_n + H \quad (23)$$

Introduction of alkane vapors such as *n*-butane, *n*-pentane, and n-hexane into the zeolite supercages partially evacuated under a vacuum of at 5×10^{-2} Torr leads to a significant increase of the lifetime of $(H_2O)_n^-$ from 1.2 to ~6 μs. This is due to the scavenging of $OH^•$ radicals by alkane molecules and the suppression of reaction 22. We have already pointed out that water cluster trapped electrons are relatively long-lived at a low water content (before the formation of cation clusters) due to the diffusion-limited nature of reactions 22 and 23. A much shorter lifetime of $(H_2O)_n^-$ in fully hydrated zeolite MCM-41 (with channels of 35 Å diameter) and a much longer lifetime in fully hydrated zeolite NaA (with α-cages of 11 Å diameter) than that in zeolites X and Y are indicative of the cage effect on the movement and reactivity of $(H_2O)_n^-$.[65]

Conclusions

The results reported in this work demonstrate that due to the confinement by zeolite structures the water in zeolites exists in the form of clusters and not as in bulk liquid. The excess electrons generated by radiolysis of the zeolite frameworks are localized either by the water clusters at high water contents or by cation clusters at low water contents, giving rise to water cluster solvated electrons and cation cluster trapped electrons, respectively. Solvation and relocation of charge-balancing cations in the presence of water tends to destroy the cation cluster trapping sites observed in completely dehydrated zeolites.

At high water contents, water cluster trapped electrons show a series of absorption spectra, which are similar to that of the hydrated electrons in liquid water and those of water cluster anions in the gas phase. Reduction in the size of water clusters by dehydration results in less solvation of excess electrons and the observed spectral red shift. The diffusivity and therefore the reactivity of water cluster trapped electrons drop significantly with the decreasing water content. It is the first experimental results in the condensed phases to clearly show how the electronic structures and properties of hydrated electrons are changed due to separation and confinement of water into nanometer clusters by the cage structure of zeolites X and Y.

When the water content is dropped too low to solvate most of the cations in the zeolite structure, cation clusters are formed and become the dominant electron-trapping sites. In between the high and low levels of hydration of zeolites, coexistence of water cluster solvated electrons and cation cluster trapped electrons and the electron transfer reaction between these two different kinds of sites are observed within a narrow range of water content. The emergence of this transition behavior during the dehydration process is mainly dependent on the Si/Al ratio of zeolites.

In contrast to the nonreactive trapping of electrons in zeolites, positive holes produced in pairs with electrons react with water, leading to the formation of hydroxyl radicals and subsequent chemistry. Reactions between $OH^•$ radicals and aromatic guest molecules are limited by the slow diffusion of $OH^•$ within the cage structure of zeolites. The high yields of hydrated electrons and hydroxyl radicals as measured in *G* values ($G = 5.8-6.0$) indicate that an efficient energy transfer from the irradiated zeolite framework to adsorbed water leads to formation of the same reactive intermediates as those produced in direct radiolysis of liquid water. As a result, the same radiation chemistry as in bulk water is observed in water clusters confined by the zeolites. The major difference lies in that the fast reactions of hydrated electrons and hydroxyl radicals normally observed in aqueous solution are highly restricted by the zeolite structure.

Acknowledgment. The authors thank the National Science Foundation for financial support of this work.

References and Notes

(1) Breck, D. W. *Zeolite Molecular Sieves: Structure, Chemistry and Use*, John Wiley & Sons: New York, 1974.
(2) Chen, N. Y. *Molecular Transport and Reaction in Zeolites: Design and Application of Shape Selective Catalysts*; VCH: New York, 1994.
(3) Barrer, R. M. *Zeolites and Clay Minerals as Sorbents and Molecular Sieves*; Academic Press: London, 1978.
(4) Bhatia, S. *Zeolite Catalysis: Principles and Applications*; CRC Press: Boca Raton, FL, 1990.
(5) Thomas, J. K. *Chem. Rev.* **1993**, *93*, 301.
(6) Calzaferri, G.; Giovanoli, R.; Kamber, I.; Shklover, V.; Nesper, R. *Res. Chem. Intermed.* **1993**, *19*, 31.
(7) Martens, L. R. M.; Grobet, P. J.; Jacobs, P. A. *Nature* **1985**, *315*, 568. Martens, L. R. M.; Grobet, P. J.; Vermerien, W. J. M.; Jacobs, P. A. *Proc. 7th Int. Zeolite Conf.* **1986**, 935. Martens, L. R. M.; Vermerien, W. J. M.; Grobet, P. J.; Jacobs, P. A. *Stud. Surf. Sci. Catal.* **1987**, *31*, 531.
(8) Edwards, P. P.; Anderson, P. A.; Thomas, J. M. *Acc. Chem. Res.* **1996**, *29*, 23.
(9) Iwamoto, M.; Maruyama, K.; Yamazoe, N.; Seiyama, T. *J. Phys. Chem.* **1977**, *81*, 622. Iwamoto, M.; Yahiro, H.; Tanda, K.; Mizuno, N.; Mine, Y.; Kagawa, S. *J. Phys. Chem.* **1991**, *95*, 3727.
(10) Kasai, P. H. *J. Chem. Phys.* **1965**, *43*, 3323. Rabo, J. A.; Angell, C. L.; Kasai, P. H.; Schomaker, V. *Discuss. Faraday Soc.* **1966**, *41*, 328. Kasai, P. H.; Bishop, Jr., R. J. *J. Phys. Chem.* **1973**, *77*, 2308. Kasai, P. H.; Bishop, Jr., R. J. In *Zeolite Chemistry and Catalysis*; Rabo, J. A., Ed.; *ACS Monogr.* **1976**, *171*, 350.
(11) Barrer, R. M.; Cole, J. F. *J. Phys. Chem. Solids* **1968**, *29*, 1755.
(12) Sun, T.; Seff, K. *Chem. Rev.* **1994**, *94*, 857.
(13) Srdanov, V. I.; Haug, K.; Metiu, H.; Stucky, G. D. *J. Phys Chem.* **1992**, *96*, 9039. Blake, N. P.; Srdanov, V. I.; Stucky, G. D.; Metiu, H. *J. Phys. Chem.* **1995**, *99*, 2127.
(14) Edwards, P. P.; Harrison, M. R.; Klinowski, J.; Ramdas, S.; Thomas, J. M.; Johnson, D. C.; Page, C. J. *J. Chem. Soc., Chem. Commun.* **1984**, 982. Harrison, M. R.; Edwards, P. P.; Klinowski, J.; Johnson, D. C.; Page, C. J. *J. Solid State Chem.* **1984**, *54*, 530. Anderson, P. A.; Singer, R. J.; Edwards, P. P. *J. Chem. Soc., Chem. Commun.* **1991**, 914. Anderson, P. A.; Edwards, P. P. *J. Chem. Soc., Chem. Commun.* **1991**, 915. Anderson, P. A.; Barr, D.; Edwards, P. P. *Angew. Chem., Int. Ed. Engl.* **1991**, *30*, 1501.
(15) Westphal, U.; Geismar, G. *Z. Anorg. Allg. Chem.* **1984**, *508*, 165. Smeulders, J. B. A. F.; Hefni, M. A.; Klaassen, A. A. K.; de Boer, E.; Westphal, U.; Geismar, G. *Zeolites* **1987**, *7*, 347. Breuer, R. E. H.; de Boer, E.; Geismar, G. *Zeolites* **1989**, *9*, 336.
(16) Xu, B.; Kevan, L. *J. Chem. Soc., Faraday Trans. 1* **1991**, *87*, 2843. Xu, B.; Kevan, L. *J. Chem. Soc., Faraday Trans. 1* **1991**, *87*, 3157. Yoon, K. B.; Kochi, J. K. *J. Chem. Soc., Chem. Commun.* **1988**, 510. Park, Y. S.; Lee, Y. S.; Yoon, K. B. *J. Am. Chem. Soc.* **1993**, *115*, 12220.
(17) Kuranova, G. A. *High Energy Chem.* **1991**, *25*, 91.
(18) Iu, K.-K.; Thomas, J. K. *J. Phys. Chem.* **1991**, 95, 506. Iu, K.-K.; Thomas, J. K. *Colloids Surf.* **1992**, *63*, 39. Liu, X.; Thomas, J. K. *Chem. Phys. Lett.* **1992**, *192*, 555. Liu, X.; Thomas, J. K. *Langmuir* **1992**, *8*, 1750. Iu, K.-K.; Liu, X.; Thomas, J. K. *J. Phys. Chem.* **1993**, *97*, 8165. Liu, X.; Iu, K.-K.; Thomas, J. K. *Chem. Phys. Lett.* **1994**, *224*, 31.
(19) Liu, X.; Iu, K.-K.; Thomas, J. K. *J. Phys. Chem.* **1994**, *98*, 13720.
(20) Liu, X.; Zhang, G.; Thomas, J. K. *J. Phys. Chem.* **1995**, *99*, 10024.
(21) Barnabas, M. V.; Trifunac, A. D. *Chem. Phys. Lett.* **1991**, *187*, 565. Barnabas, M. V.; Trifunac, A. D. *Chem. Phys. Lett.* **1992**, *193*, 298. Barnabas, M. V.; Werst, D. W.; Trifunac, A. D. *Chem. Phys. Lett.* **1993**, *204*, 435. Barnabas, M. V.; Werst, D. W.; Trifunac, A. D. *Chem. Phys. Lett.* **1993**, *206*, 21. Cromack, K. R.; Werst, D. W.; Barnabas, M. V.; Trifunac, A. D. *Chem. Phys. Lett.* **1994**, *218*, 485. Werst, D. W.; Tartakovsky, E. E.; Piocos, E. A.; Trifunac, A. D. *J. Phys. Chem.* **1994**, *98*, 10249.
(22) Haberland, H.; Ludewigt, C.; Schindler, H. G.; Worsnop, D. R. *J. Phys. Chem.* **1984**, *81*, 3742.

(23) Coe, J. V.; Lee, G. H.; Eaton, J. G.; Arnold, S. T.; Sarkas, H. W.; Bowen, K. H.; Ludewigt, C.; Haberland, H.; Worsnop, D. R. *J. Chem. Phys.* **1990**, *92*, 3980. Haberland, H.; Bowen, K. H. *Springer Ser. Chem. Phys.* **1994**, *56*, 134.

(24) Lavrich, D. J.; Campagnola, P. J.; Johnson, M. A. In *NATO ASI Series Vol. 326, Linking the Gaseous and Condensed Phases of Matter;* Christophorou, L. G., et al., Eds.; D. Reidel: Boston, 1994; p 183. Campagnola, P. J.; Lavrich, D. J.; DeLuca, M. J.; Johnson, M. A. *J. Chem. Phys.* **1991**, *94*, 5240.

(25) Hart, E. J.; Anbar, M. *The Hydrated Electron*; Wiley-Interscienece: New York, 1970; p 42 and references therein.

(26) Feng, D. F.; Keven, L. *Chem. Rev.* **1980**, *80*, 1.

(27) Zagorski, Z. P. *J. Phys. Chem.* **1986**, *90*, 957; **1987**, *91*, 734, 972.

(28) Schwartz, B. J.; Rossky, P. J. *J. Phys. Chem.* **1994**, *98*, 4489. Keszei, E.; Murphrey, T. H.; Rossky, P. J. *J. Phys. Chem.* **1995**, *99*, 22.

(29) Kimura, Y.; Alfano, J. C.; Walhout, P. K.; Barbara, P. F. *J. Phys. Chem.* **1994**, *98*, 3450.

(30) Kühl, G. H. *Zeolites* **1986**, *6*, 161.

(31) Meier, W. M.; Olson, D. H. *Atlas of Zeolite Types*; Butterworths: London, 1987.

(32) Gramlich, V.; Meier, W. M. *Z. Kristallogr.* **1971**, *133*, 134.

(33) Solar, S.; Solar, W.; Getoff, N. *J. Chem. Soc., Faraday Trans. 1* **1982**, *78*, 2467.

(34) Ogg, R. A., Jr. *Phys. Rev.* **1946**, *69*, 668.

(35) Jortner, J. *J. Chem. Phys.* **1959**, *30*, 839. Jortner, J.; Rice, S. A.; Wilson, E. G. In *Metal Ammonia Solutions*; Lepoutre, G., Sienko, M. J., Eds.; W. A. Benjamin: New York, 1964. Copeland, D. A.; Kestner, N. R.; Jortner, J. *J. Chem. Phys.* **1970**, *53*, 1189. Jortner, J. *Ber. Bunsen-Ges. Phys. Chem.* **1971**, *75*, 646.

(36) Schnitker, J.; Rossky, P. J. *J. Phys. Chem.* **1988**, *92*, 4277 and references therein.

(37) Barnett, R. N.; Landman, U.; Cleveland, C. L. Jortner, J. *Chem. Phys. Lett.* **1988**, *145*, 382; *J. Chem. Phys.* **1988**, *88*, 4429.

(38) Barnett, R. N.; Landman, U.; Nitzan, A. *J. Chem. Phys.* **1988**, *89*, 2242. Barnett, R. N.; Landman, U.; Makov, G.; Nitzan, A. *J. Chem. Phys.* **1990**, *93*, 6226

(39) Barrer, R. M. *Zeolites and Clay Minerals as Sorbents and Molecular Sieves*; Academic Press: London, 1978; p 121.

(40) Wong, M.; Gratzel, M.; Thomas, J. K. *Chem. Phys. Lett.* **1975**, *30*, 329. Wong, M.; Thomas, J. K.; Nowak, T. *J. Am. Chem. Soc.* **1977**, *99*, 4730.

(41) Pileni, M. P.; Hickel, B.; Ferradini, C.; Pucheault, J. *Chem. Phys. Lett.* **1982**, *92*, 308.

(42) Kreitus, I. V. *J. Phys. Chem.* **1985**, *89*, 1987.

(43) Van Dun, J. J.; Motier, W. J. *Zeolites* **1987**, *7*, 528.

(44) Motier, W. J. *Compilation of Extra Framework Sites in Zeolites*; Butterworth Scientific Ltd.: London, 1982; p 19.

(45) Rice, S. A. *Comprehensive Chemical Kinetics: Vol.25, Diffusion-limited Reactions*; Bamford, C. H., Tipper, C. F. H., Compton, R. G., Eds.; Elsevier: Amsterdam, 1985; Chapter 2.

(46) See ref 25, p 57.

(47) Schmidt, K. H.; Han, P.; Bartels, D. M. *J. Phys. Chem.* **1992**, *96*, 199.

(48) Schnitker, J.; Rossky, P. J. *J. Phys. Chem.* **1989**, *93*, 6965.

(49) Barnett, R. N.; Landman, U.; Nitzan, A. *J. Chem. Phys.* **1990**, *93*, 8187.

(50) See ref 25, p 186.

(51) Karger, J. *Z. Phys. Chem. (Leipzig)* **1971**, *248*, 27.

(52) Avery, E. C.; Remko, J. R.; Samller, B. *J. Chem. Phys.* **1968**, *49*, 951.

(53) Wertz, J. E.; Bolton, J. R. *Electron Spin Resonance: Elementary Theory and Practical Applications*; Chapman Hall: New York, 1986.

(54) Zhang, G. Radiation Induced Processes in Polymer Films and on Silica Surfaces. Ph.D. Dissertation, University of Notre Dame, Notre Dame, IN, 1996; Chapter 6.

(55) Aoki, M.; Nakazato, C.; Masuda, T. *Bull. Chem. Soc. Jpn.* **1988**, *61*, 1899.

(56) Liu, X.; Thomas, J. K. *J. Chem. Soc., Faraday Trans.* **1995**, *91*, 759.

(57) Zhang, G.; Thomas, J. K. Unpublished data.

(58) Barber, D. J.; Thomas, J. K. *Radiat. Res.* **1978**, *74*, 51.

(59) Shiromaru, H.; Shinohara, H.; Washida, N.; Yoo, H.-S.; Kimura, K. *Chem. Phys. Lett.* **1987**, *141*, 7. Ahmed, M.; Apps, C. J.; Hughes, C.; Whitehead, J. C. *J. Phys. Chem.* **1994**, *98*, 12530. Barnett, R. N.; Landman, U. *J. Phys. Chem.* **1995**, *99*, 17305.

(60) Spinks, J. W. T.; Woods, R. J. *An Introduction to Radiation Chemistry*, 2nd ed.; John Wiley & Sons: New York, 1976.

(61) Iwata, A.; Nakashima, N.; Izawa, Y.; Yamanaka, C. *Chem. Lett.* **1993**, *11*, 1939.

(62) Posey, L. A.; Deluca, M. J.; Campagnola, P. J.; Johnson, M. A. *J. Phys. Chem.* **1989**, *83*, 1178. Arnold, S. A.; Morris, R. A.; Viggiano, A. A.; Johnson, M. A. *J. Phys. Chem.* **1996**, *100*, 2900.

(63) Michael, B. D.; Hart, E. J. *J. Phys. Chem.* **1970**, *74*, 2878. Krauss, M.; Osman, R. *Chem. Phys. Lett*. **1995**, *239*, 258.

(64) Solar, S.; Solar, W., Getoff, N. *J. Chem. Soc., Faraday Trans. 1* **1985**, *81*, 1101.

(65) Liu, X.; Zhang, G.; Thomas, J. K. Unpublished results.